Broadband Spectral Numerical Green's Function for Electromagnetic Analysis of Inhomogeneous Objects

Hui H. Gan, Qi I. Dai, Tian Xia, Weng Cho Chew, *Fellow, IEEE*, and Chao-Fu Wang, *Senior Member, IEEE*

***Abstract*—In this letter, we present a novel and efficient broadband spectral numerical Green's function (S-NGF) for inhomogeneous region. The proposed S-NGF is formulated in terms of the matrices that are obtained by the finite-element method (FEM). By performing modal analysis to FEM matrices, the proposed S-NGF is encapsulated by a series of resonant solenoidal modes where the operating frequency is embedded in the expansion coefficients. Besides, the convergence of the series of resonant solenoidal modes can be greatly accelerated by performing an extraction at one low wavenumber. The S-NGF can be rapidly reconstructed at different frequencies when it is integrated into the surface integral equation for inhomogeneous object modeling. The proposed algorithm is easy to implement, and well suited for the design and optimization of inhomogeneous electromagnetic structures, where fast solutions at massive frequencies are called for. The numerical examples demonstrate the efficiency and accuracy of the proposed scheme.**

***Index Terms*—Eigenanalysis, frequency sweep, low wavenumber extraction (LWNE), numerical Green's function (NGF), wideband spectral representation.**

I. Introduction

DESIGN of electromagnetic (EM) devices such as antennas, microwave circuits, and cavity resonators require one to carry out EM analysis for inhomogeneous media at massive frequencies, where efficient and accurate broadband algorithms are desired [1]–[3]. The surface integral equation has been widely used in analysis of EM devices with piecewise media [4]–[6]. However, the SIE has difficulty in dealing with inhomogeneous media since the corresponding Green's function has no closed-form expression. Differential equation solvers, e.g., the finite difference method and the finite element method (FEM), have the flexibility in handling complicated inhomogeneity. Recently, numerical Green's function (NGF) obtained by FEM was introduced into the SIE for inhomogeneous media modeling [7]. When the scheme is applied to broadband simulations, NGFs have to be solved at each frequency which leads to low computational efficiency.

Analytic broadband Green's function expression was proposed over three decades ago, termed as boundary integral-resonant mode expansion (BI-RME), for modal analysis of strongly perturbed rectangular or circular metallic waveguides [8], [9]. The innovative idea in BI-RME is to represent the Green's function of the problem as a sum of a quasistatic frequency-independent kernel and a series consisting of 2-D resonant modes of the unperturbed waveguide [10]. This Green's function is invoked in the boundary integral scheme with the method of moments (MoM) to form a linear matrix eigenvalue problem (EVP) with eigenvalues as the unknown resonant wavenumbers. BI-RME was later extended to the 3-D version with boxed external cavities used to investigate waveguide circuits including dielectric elements [11]. More recently, BI-RME is modified for the calculation of band diagrams and low frequency dispersion relations of periodic scatterers, where a low wavenumber extraction (LWNE) is utilized to expedite the convergence of the series expansion [12], [13]. However, the implementation of BI-RME seems more involved than the conventional MoM code for the analytical calculation of some tedious singular integrals [14]. Moreover, these schemes are limited to simple waveguide or cavity geometries where resonant modes are analytically available.

The motivation of this letter is to formulate a broadband NGF that can be applied to general inhomogeneous media with an arbitrary shape. Invoking mode expansion, the proposed spectral-numerical Green's function (S-NGF) of inhomogeneous media is encapsulated by a series of the eigenmode which are resulted from FEM discretization of an arbitrarily shaped and material-loaded region. Since frequency is embedded in the expansion coefficients, S-NGF can be reconstructed cheaply when frequency is changed. Motivated by [12] and [13], the convergence of the series formed by resonant solenoidal modes is greatly accelerated with an extraction at one low wavenumber. Besides, the contribution from the spurious direct current (dc) or irrotational modes is treated as a whole by solving a simple Poisson equation. This reduced modal picture can be used for model order reduction of complicated resonating systems [15], [16]. This proposed approach is fairly easy to implement as only the manipulation of FEM matrices is required, which

Manuscript received February 17, 2020; revised March 30, 2020; accepted April 13, 2020. Date of publication April 20, 2020; date of current version July 7, 2020. This work was supported in part by the NSF ECCS 169195, in part by ANSYS Inc. PO37497, in part by AF Sub RRI PO0539, in part by the George and Ann Fisher Professorship at the University of Illinois, and in part by the Distinguished Professorship at Purdue University. *(Corresponding author: Hui H. Gan.)*

Hui H. Gan, Qi I. Dai, and Tian Xia are with the Department of Electrical and Computer Engineering, University of Illinois at Urbana−Champaign, Urbana, IL 61801 USA (e-mail: huigan2@illinois.edu; daiqi@illinois.edu; tianxia3@illinois.edu).

Weng Cho Chew is with the School of Electrical and Computer Engineering, Purdue University, West Lafayette, IN 47907 USA (e-mail: wcchew@purdue.edu).

Chao-Fu Wang Chew is with the Temasek Laboratories, National University of Singapore, Singapore 117411 (e-mail: cfwang@nus.edu.sg).

Digital Object Identifier 10.1109/LAWP.2020.2988475

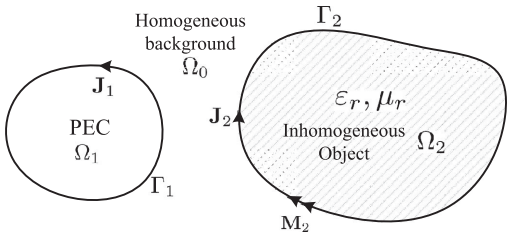

Fig. 1. PEC object with background.

avoids the complicated singular integrals. In this letter, we only consider lossless dielectric object, but the proposed S-NGF can be extended to lossy or magnetic material easily.

II. Formulation

A. NGF of Inhomogeneous Media

As shown in Fig. 1, a perfect electric conductor (PEC) object Ω_1 and an inhomogeneous object Ω_2 are placed under a homogeneous background Ω_0, where $\mathbf{J}_1$ is the equivalence electric current on surface Γ_1, $\mathbf{J}_2$ and $\mathbf{M}_2$ are the equivalence electric current and magnetic current on surface Γ_2, respectively. The conventional SIE scheme has difficulty in solving this problem due to the lack of closed-form Green's function for inhomogeneous object [17]. The NGF is an alternative option to bypass the issue.

When an arbitrary current source $\mathbf{J}_a$ is introduced into Ω_2, the electric field in Ω_2 is subject to the governing wave equation as

$$\nabla \times \nabla \times \mathbf{E}(\mathbf{r}) - k_0^2 \varepsilon_r(\mathbf{r}) \mathbf{E}(\mathbf{r}) = i\omega\mu_0 \mathbf{J}_a, \quad \mathbf{r} \in \Omega_2 \tag{1}$$

where $k_0 = \omega\sqrt{\varepsilon_0\mu_0}$, ω is the frequency and ε_r denotes the relative permittivity. Only the nonmagnetic and lossless isotropic material is considered in this letter. Different boundary conditions can be applied to Γ_2 when solving for the NGF [7]. In this letter, the boundary is assumed to be a magnetic wall, we have $\hat{n} \times \mathbf{H} = 0$ where $\hat{n}$ is the unit normal vector pointing outwards from the surface Γ_2.

Equation (1) is discretized by FEM due to its versatility in handling complicated material properties. The domain Ω_2 is partitioned into many tetrahedral elements, and the fields are approximated with N_2 edge element basis functions [18] (Whitney 1-forms) $\mathbf{N}_i$ as

$$\mathbf{E}(\mathbf{r}) = \sum_{i=1}^{N_2} \mathbf{N}_i(\mathbf{r}) e_i = \overline{\mathbf{N}}^t(\mathbf{r}) \cdot \boldsymbol{e} \tag{2}$$

where N_2 is the total number of edges in Ω_2, $\overline{\mathbf{N}}^t(\mathbf{r}) = [\mathbf{N}_1(\mathbf{r}), \mathbf{N}_2(\mathbf{r}), \ldots, \mathbf{N}_{N_2}(\mathbf{r})]$; $\boldsymbol{e}$ is a column vector containing expansion coefficients e_i as entries. Thus, by applying the Galerkin's procedure, (1) results in

$$(\overline{\mathbf{S}} - k_0^2 \overline{\mathbf{T}}) \cdot \boldsymbol{e} = \boldsymbol{f} \tag{3}$$

where

$$[\overline{\mathbf{S}}]_{ij} = \langle \nabla \times \mathbf{N}_i, \nabla \times \mathbf{N}_j \rangle_{\Omega_2} \tag{4}$$

$$[\overline{\mathbf{T}}]_{ij} = \langle \mathbf{N}_i, \varepsilon_r \mathbf{N}_j \rangle_{\Omega_2} \tag{5}$$

$$[\boldsymbol{f}]_i = \langle \mathbf{N}_i, i\omega\mu_0 \mathbf{J}_a \rangle_{\Omega_2} \tag{6}$$

where the inner product is defined as $< \mathbf{h},\ \mathbf{g} >_{\mathcal{D}} = \int_{\mathcal{D}} \mathbf{h} \cdot \mathbf{g}\ d\mathbf{r}$. After solving (3) for $\boldsymbol{e}$, $\mathbf{E}(\mathbf{r})$ can be written as

$$\mathbf{E}(\mathbf{r}) = \overline{\mathbf{N}}^t(\mathbf{r}) \cdot \left(\overline{\mathbf{S}} - k_0^2 \overline{\mathbf{T}}\right)^{-1} \cdot \boldsymbol{f}. \tag{7}$$

Therefore, the NGF of object Ω_2, which maps the arbitrary current source to the electric field in the region, can be expressed in terms of FEM vector basis as [7]

$$\overline{\mathbf{G}}_2(\mathbf{r}, \mathbf{r}') = \overline{\mathbf{N}}^t(\mathbf{r}) \cdot \overline{\boldsymbol{\mathcal{G}}}(k_0) \cdot \overline{\mathbf{N}}(\mathbf{r}') \tag{8}$$

where

$$\overline{\boldsymbol{\mathcal{G}}}(k_0) = \left(\overline{\mathbf{S}} - k_0^2 \overline{\mathbf{T}}\right)^{-1}. \tag{9}$$

To analyze the problem in Fig. 1, S-NGF is integrated into the SIE of interior inhomogeneous region Ω_2 [7] and the final equations are written as

$$\mathcal{L}_0 \cdot \mathbf{J}_1 + \mathcal{L}_0 \cdot \mathbf{J}_2 + \mathcal{K}_0 \cdot \mathbf{M}_2 = -\mathbf{E}_{\text{inc}}(\mathbf{r}), \quad \mathbf{r} \in \Gamma_1^- \tag{10}$$

$$\mathcal{L}_0 \cdot \mathbf{J}_1 + \mathcal{L}_0 \cdot \mathbf{J}_2 + \mathcal{K}_0 \cdot \mathbf{M}_2 = -\mathbf{E}_{\text{inc}}(\mathbf{r}), \quad \mathbf{r} \in \Gamma_2^- \tag{11}$$

$$\mathcal{L}_1 \cdot \mathbf{J}_2 + \mathcal{K}_1 \cdot \mathbf{M}_2 = 0, \qquad \mathbf{r} \in \Gamma_2^+ \tag{12}$$

where superscript $-$ and $+$ indicate the interior and exterior side of surface, respectively. The operators are defined as

$$\mathcal{L}_0 \cdot \mathbf{J}_i = i\omega\mu_0 \int_S d\mathbf{r}'\ \overline{\mathbf{G}}_0(\mathbf{r}, \mathbf{r}') \cdot \mathbf{J}_i(\mathbf{r}') \tag{13}$$

$$\mathcal{K}_0 \cdot \mathbf{M}_2 = \int_S d\mathbf{r}'\ \nabla \times \overline{\mathbf{G}}_0(\mathbf{r}, \mathbf{r}') \cdot \mathbf{M}_2(\mathbf{r}') \tag{14}$$

$$\mathcal{L}_1 \cdot \mathbf{J}_i = i\omega\mu_0 \overline{\mathbf{N}}^t(\mathbf{r}) \cdot \overline{\boldsymbol{\mathcal{G}}}(k_0) \cdot \langle \overline{\mathbf{N}}(\mathbf{r}),\ \mathbf{J}_i \rangle_S \tag{15}$$

$$\mathcal{K}_1 \cdot \mathbf{M}_2 = \overline{\mathbf{N}}^t(\mathbf{r}) \cdot \overline{\boldsymbol{\mathcal{G}}}(k_0) \cdot \langle \nabla' \times \overline{\mathbf{N}}(\mathbf{r}),\ \mathbf{M}_2 \rangle_S \tag{16}$$

where $i = 1, 2$ and $\overline{\mathbf{G}}_0(\mathbf{r}, \mathbf{r}')$ is homogeneous Green's function with closed-form expression. Model-order reduction method can be applied to expedite the calculation of interaction between object Ω_1 and Ω_2 [17].

However, when frequency sweep is required in the application, solving for the NGF in (8) is expensive because it is frequency dependent and the matrix inversion in (9) has to be performed at each frequency. To overcome the obstacle, the spectral representation of $\overline{\boldsymbol{\mathcal{G}}}(k_0)$ is adopted where this NGF is expanded by a series of eigenmodes of the inhomogeneous domain. The S-NGF is a combination of frequency-independent matrices with frequency embedded in the expansion coefficients, thus it can be calculated cheaply when frequency is changed.

B. Spectral Numerical Green's Function

The wave equation (1) can be rewritten as an eigenmode equation, where the wavenumbers k_n^0 and modal fields $\mathbf{E}_n^0$ in

Ω_2 are subject to the source-free governing equation as

$$\nabla \times \nabla \times \mathbf{E}_n^0(\mathbf{r}) = \left(k_n^0\right)^2 \varepsilon_r(\mathbf{r}) \mathbf{E}_n^0(\mathbf{r}), \quad \mathbf{r} \in \Omega_2. \tag{17}$$

After FEM discretization, (17) results in

$$\overline{\mathbf{S}} \cdot \mathbf{e}_n^0 = \left(k_n^0\right)^2 \overline{\mathbf{T}} \cdot \mathbf{e}_n^0. \tag{18}$$

The eigensolutions of (18) can be categorized into two classes. The first class are resonant or solenoidal modes corresponding to nonvanishing eigenvalues, which is written as

$$\overline{\mathbf{S}} \cdot \overline{\mathbf{U}} = \overline{\mathbf{T}} \cdot \overline{\mathbf{U}} \cdot \overline{\mathbf{\Lambda}} \tag{19}$$

where $\overline{\mathbf{U}}$ is a matrix containing all solenoidal modes as column vectors; $\overline{\mathbf{\Lambda}}$ is a diagonal matrix given by

$$\overline{\mathbf{\Lambda}} = \operatorname{diag}\left[\left(k_1^0\right)^2, \left(k_2^0\right)^2, \ldots\right], \quad k_n^0 \neq 0. \tag{20}$$

After normalization, the orthogonality conditions can be obtained as

$$\overline{\mathbf{U}}^t \cdot \overline{\mathbf{S}} \cdot \overline{\mathbf{U}} = \overline{\mathbf{\Lambda}} \tag{21}$$

$$\overline{\mathbf{U}}^t \cdot \overline{\mathbf{T}} \cdot \overline{\mathbf{U}} = \overline{\mathbf{I}} \tag{22}$$

where $\overline{\mathbf{I}}$ is an identity matrix. The second class are irrotational or spurious dc modes corresponding to the zero eigenvalues. They form the null-space of $\overline{\mathbf{S}}$, which is essentially the gradient projector $\overline{\mathbf{P}}$ satisfying $\nabla \times [(\overline{\mathbf{P}} \cdot \boldsymbol{e})^t \cdot \overline{\mathbf{N}}(\mathbf{r})] = 0$. Here, $\overline{\mathbf{P}}$ is a sparse matrix containing 1, -1, and 0 only. Operating the Whitney 1-forms $\overline{\mathbf{N}}(\mathbf{r})$ with $\overline{\mathbf{P}}$ is considered as a gradient of scalar function, which is the null space of the curl operator. It can be easily constructed such that $\overline{\mathbf{P}}^t \cdot \overline{\mathbf{S}} = 0$ and $\overline{\mathbf{S}} \cdot \overline{\mathbf{P}} = 0$ [19].

The solution to (3) can be expanded with these eigenmodes as they form a complete space, or

$$\boldsymbol{e} = \left(\overline{\mathbf{S}} - k_0^2 \overline{\mathbf{T}}\right)^{-1} \cdot \boldsymbol{f} = \overline{\mathbf{U}} \cdot \boldsymbol{a} + \overline{\mathbf{P}} \cdot \boldsymbol{b} \tag{23}$$

where $\boldsymbol{a}$ and $\boldsymbol{b}$ are the vectors of modal expansion coefficients. By invoking the orthogonality conditions between the two classes of modes that

$$\overline{\mathbf{U}}^t \cdot \overline{\mathbf{T}} \cdot \overline{\mathbf{P}} = \overline{\mathbf{0}} \tag{24}$$

the coefficients can be computed as

$$\boldsymbol{a} = \left(\overline{\mathbf{\Lambda}} - k_0^2 \overline{\mathbf{I}}\right)^{-1} \cdot \overline{\mathbf{U}}^t \cdot \boldsymbol{f} \tag{25}$$

and

$$\boldsymbol{b} = -\frac{1}{k_0^2} \left(\overline{\mathbf{P}}^t \cdot \overline{\mathbf{T}} \cdot \overline{\mathbf{P}}\right)^{-1} \cdot \overline{\mathbf{P}}^t \cdot \boldsymbol{f}. \tag{26}$$

After substituting (25) and (26) into (23), the $\overline{\boldsymbol{\mathcal{G}}}(k_0)$ is expanded by the eigenmode as

$$\begin{aligned} \overline{\boldsymbol{\mathcal{G}}}(k_0) = {} & \overline{\mathbf{U}} \cdot \left(\overline{\mathbf{\Lambda}} - k_0^2 \overline{\mathbf{I}}\right)^{-1} \cdot \overline{\mathbf{U}}^t \\ & - \frac{1}{k_0^2} \overline{\mathbf{P}} \cdot \left(\overline{\mathbf{P}}^t \cdot \overline{\mathbf{T}} \cdot \overline{\mathbf{P}}\right)^{-1} \cdot \overline{\mathbf{P}}^t. \end{aligned} \tag{27}$$

On the right-hand side of (27), the first term is the series formed by solenoidal modes which can be truncated with a limited error as it converges as $1/(k_n^0)^2$. For the second term, it is obvious that the contribution of the irrotational modes is treated as a whole. In addition, $\overline{\mathbf{P}}$ and $\overline{\mathbf{P}}^t$ correspond to the discrete gradient and divergence operators, respectively; $(\overline{\mathbf{P}}^t \cdot \overline{\mathbf{T}} \cdot \overline{\mathbf{P}})^{-1}$ is equivalent to solving a Poisson's equation.

Furthermore, the efficiency of the scheme can be enhanced by reducing the number of solenoidal modes used in the spectral representation. This is achieved by the S-NGF extraction at one low wavenumber k_L as [12]

$$\begin{aligned} \overline{\boldsymbol{\mathcal{G}}}(k_0) = {} & \overline{\boldsymbol{\mathcal{G}}}(k_L) + \frac{1}{k_L^2} \overline{\mathbf{H}} - \frac{1}{k_0^2} \overline{\mathbf{H}} \\ & + (k_0^2 - k_L^2) \overline{\mathbf{U}} \cdot \left(k_L^2 \overline{\mathbf{I}} - \overline{\mathbf{\Lambda}}\right)^{-1} \cdot \left(k_0^2 \overline{\mathbf{I}} - \overline{\mathbf{\Lambda}}\right)^{-1} \cdot \overline{\mathbf{U}}^t \end{aligned} \tag{28}$$

where

$$\overline{\mathbf{H}} = \overline{\mathbf{P}} \cdot \left(\overline{\mathbf{P}}^t \cdot \overline{\mathbf{T}} \cdot \overline{\mathbf{P}}\right)^{-1} \cdot \overline{\mathbf{P}}^t. \tag{29}$$

The low wavenumber k_L is much lower than the wavenumber of interest, which is set to be $1/10$ of the smallest wavenumber in frequency sweep in this letter. The series of solenoidal modes converges as $1/(k_n^0)^4$ after the LWNE is applied. After performing LWNE, smaller number of modes is needed to expand the NGF with the same accuracy compared to the formulation without LWNE in (27).

When the tetrahedral mesh is used for the discretization where M nodes and N edges are generated, both FEM matrices $\overline{\mathbf{S}}$ and $\overline{\mathbf{T}}$ are $N \times N$; the dimensions of $\overline{\mathbf{P}}$, $\overline{\mathbf{U}}$, and $\overline{\mathbf{\Lambda}}$ are $N \times M$ and $N \times K$, and $K \times K$, respectively, where $K = N - M$. However, for a given range of k_0, the series can be approximated with K_s solenoidal modes, where K_s is a small number. Accordingly, the matrices in the series are truncated to be $\overline{\mathbf{U}}_s$, $\overline{\mathbf{\Lambda}}_s$, and $\overline{\mathbf{I}}_s$, with the dimensions as $N \times K_s$, $K_s \times K_s$, and $K_s \times K_s$, respectively. As shown in (28), $\overline{\boldsymbol{\mathcal{G}}}(k_L)$, $\overline{\mathbf{H}}$, and $\overline{\mathbf{U}}$ only need to be calculated once when frequency sweep is required and they can be reused when frequency is changed.

III. Numerical Results

To show the efficiency and accuracy of the proposed scheme, two examples are studied. We first study the accuracy and convergence characteristics of S-NGF when it is truncated with a limited number of eigenmodes. In order to validate the efficiency of the proposed scheme, S-NGF is integrated with SIE to construct the impedance matrix for characteristic mode analysis (CMA) when frequency sweep is required.

A. Accuracy of S-NGF

The accuracy of the S-NGF is examined in the following example as shown in Fig. 2, where a conducting sphere is placed close to a three-layer dielectric background. The relative permittivity of the three layers are 2.0, 4.0, and 2.0, respectively. The dimensions of the structure are shown in the Fig. 2, where the sphere is centered at origin. In FEM discretization, the total number of edges in the inhomogeneous dielectric background is 7778.

First of all, the general EVP in (17) is solved and a number of 110 solenoidal modes with the lowest nonzero eigenvalues are

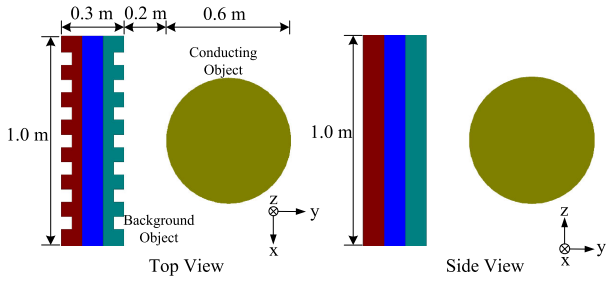

Fig. 2. Inhomogeneous background with a PEC sphere.

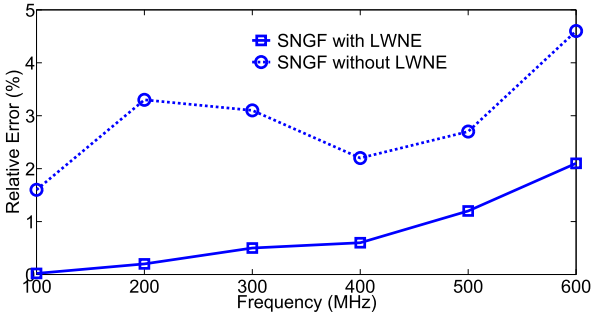

Fig. 3. Approximation errors of S-NGF.

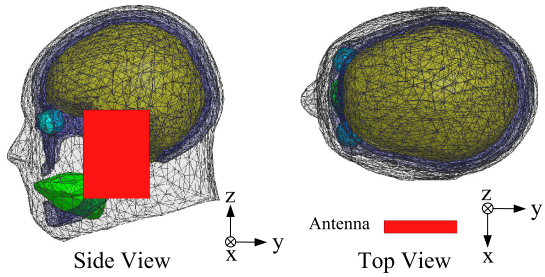

Fig. 4. Human head structure with antenna.

TABLE I
CHARACTERISTIC VALUES (CV) COMPARISONS

CV index	1	2	3	4	5
#1 w/o (0.8)	−4.07	−8.36	21.34	−67.72	79.46
#1 w/o (1.0)	−1.97	−4.06	11.89	−38.07	43.88
#1 w/o (1.2)	−0.86	−2.22	7.54	−24.85	27.56
#1 w/ (0.8)	−6.30	−14.87	22.06	−48.53	50.96
#1 w/ (1.0)	−1.78	−4.07	6.47	−25.62	31.34
#1 w/ (1.2)	−0.98	−2.45	7.63	−19.03	24.64

precalculated. In this letter, Intel Math Kernel Library eigensolver is used to search for the eigenvalues and eignvectors in a range given by the user. Frequency sweep from 100 to 600 MHz with a step of 100 MHz is implemented where the S-NGF at each frequency is constructed promptly by the 110 modes. Both of the S-NGF without and with LWNE are calculated by (27) and (28), respectively. The low wavenumber k_L is chosen to be 1. The S-NGFs are compared to the NGF calculated by the representation in (8). The relative errors at different frequencies are shown in the Fig. 3, where the relative error is defined as

$$\left\|\overline{\mathcal{G}}_{\mathrm{SNGF}}(k_0) - \overline{\mathcal{G}}_{\mathrm{NGF}}(k_0)\right\| / \left\|\overline{\mathcal{G}}_{\mathrm{NGF}}(k_0)\right\|. \tag{30}$$

As shown in the Fig. 3, the total error of S-NGF approximation with 110 eigenmodes is less than 5% in the frequency range. The error can be controlled by the truncation number of the expanding modes which is determined by its eigenvalues. Besides, the S-NGF with LWNE converges much faster than the S-NGF without LWNE at all frequency points. The error increases with frequency because higher frequency needs more modes to expand. For $\overline{\mathcal{G}}_{\mathrm{NGF}}(k_0)$, solving (9) directly with LU decomposition needs 18 s at each frequency point. In the S-NGF method, the total time of precalculating the 110 modes is 48 s, but it only needs to be generated once at 100 MHz. The time of generating S-NGFs at the rest frequency points is less than one second.

B. Antenna With Inhomogeneous Background

Wu [20] has studied the application of CMA for antenna with homogeneous background by SIE. In this example, the proposed S-NGF is applied to its proposed scheme for CMA of conducting objects with inhomogeneous media. The analysis can be remarkably accelerated by the application of S-NGF when frequency sweep is required.

As shown in the Fig. 4, a conducting plate antenna is placed beside an inhomogeneous human head structure [21]. The dimension of the plate is $L_x \times L_y \times L_z = 10 \times 60 \times 80$ mm. Since lossless materials are considered in this letter, the relative permittivity for the fat, eyeballs, tongue, brain, and bone are set to be 5.0, 8.0, 6.0, 3.0, and 9.0, respectively. The total number of edges on the dielectric surface and antenna surface are 3180 and 3546, respectively. There are 60 370 edges in the inhomogeneous dielectric region. Frequency sweep is applied from 0.8 to 1.2 GHz with a step of 0.1 GHz.

The computation time of different steps are listed as follows.

1) Precalculating the S-NGF eigenvalues and generating the frequency independent matrices with 45 modes: 1563 s.
2) Generating the impedance matrix of antenna with inhomogeneous background at each frequency: 10 s.
3) Calculating the NGF directly with (9) at each frequency: 1400 s.

Therefore, the total time of calculating S-NGF at all five frequencies is 1603 s, compared to 7000 s when generating NGF directly without S-NGF.

The characteristic values of the five important modes at 0.8, 1.0, and 1.2 GHz with (w/) the presence of background are listed in the Table I. The characteristic values of the antenna without (w/o) the presence of background are also shown in Table 1 for comparisons.

IV. CONCLUSION

In this letter, we proposed a broadband S-NGF scheme which is applicable to the SIE for inhomogeneous media analysis. The fast-converging spectral NGF with LWNE is suitable for the applications when modelings at a massive frequencies are required. The examples demonstrate the efficiency and accuracy of our work.

REFERENCES

[1] T. Xia, L. L. Meng, Q. S. Liu, H. H. Gan, and W. C. Chew, "A low-frequency stable broadband multilevel fast multipole algorithm using plane wave multipole hybridization," *IEEE Trans. Antennas Propag.*, vol. 66, no. 11, pp. 6137–6145, Nov. 2018.

[2] Q. I. Dai, Q. S. Liu, H. U. Gan, and W. C. Chew, "Combined field integral equation-based theory of characteristic mode," *IEEE Trans. Antennas Propag.*, vol. 63, no. 9, pp. 3973–3981, Sep. 2015.

[3] T. Xia *et al.*, "An integral equation modeling of lossy conductors with the enhanced augmented electric field integral equation," *IEEE Trans. Antennas Propag.*, vol. 65, no. 8, pp. 4181–4190, Aug. 2017.

[4] S. M. Rao, D. R. Wilton, and A. W. Glisson, "Electromagnetic scattering by surfaces of arbitrary shape," *IEEE Trans. Antennas Propag.*, vol. AP-30, no. 3, pp. 409–418, May 1982.

[5] J. S. Zhao and W. C. Chew, "Integral equation solution of Maxwell's equations from zero frequency to microwave frequencies," *IEEE Trans. Antennas Propag.*, vol. 48, no. 10, pp. 1635–1645, Oct. 2000.

[6] F. P. Andriulli *et al.*, "A multiplicative calderon preconditioner for the electric field integral equation," *IEEE Trans. Antennas Propag.*, vol. 56, no. 8, pp. 2398–2412, Aug. 2008.

[7] H. H. Gan, Q. Dai, T. Xia, L. Sun, and W. C. Chew, "Hybridization numerical Green's function of anisotropic inhomogeneous media with surface integral equation," *Microw. Opt. Technol. Lett.*, vol. 59, no. 7, pp. 1781–1786, 2017.

[8] G. Conciauro, M. Bressan, and C. Zuffada, "Waveguide modes via an integral equation leading to a linear matrix eigenvalue problem," *IEEE Trans. Microw. Theory Techn.*, vol. MTT-32, no. 11, pp. 1495–1504, Nov. 1984.

[9] G. Conciauro, M. Guglielmi, and R. Sorrentino, *Advanced Modal Analysis*. Hoboken, NJ, USA: Wiley, 2000.

[10] P. Arcioni, M. Bozzi, M. Bressan, G. Conciauro, and L. Perregrini, "The BI-RME method: An historical overview," in *Proc. Int. Conf. Numer. Electromagn. Model. Optim. RF, Microw., Terahertz Appl.*, 2014, pp. 1–4.

[11] J. Gil *et al.*, "Full-wave analysis and design of dielectric-loaded waveguide filters using a state- space integral-equation method," *IEEE Trans. Microw. Theory Techn.*, vol. 57, no. 1, pp. 109–120, Jan. 2009.

[12] L. Tsang and S. Huang, "Broadband Green's function with low wavenumber extraction for arbitrary shaped waveguide with applications to modeling of vias in finite power/ground plane," *Prog. Electromagn. Res.*, vol. 152, pp. 105–125, 2015.

[13] L. Tsang and S. Tan, "Calculations of band diagrams and low frequency dispersion relations of 2D periodic dielectric scatterers using broadband Green's function with low wavenumber extraction (BBGFL)," *Opt. Express*, vol. 24, pp. 945–965, 2016.

[14] P. Arcioni, M. Bressan, and L. Perregrini, "On the evaluation of the double surface integrals arising in the application of the boundary integral method to 3-D problems," *IEEE Trans. Microw. Theory Techn.*, vol. 45, no. 3, pp. 436–439, Mar. 1997.

[15] Q. I. Dai, Y. H. Lo, W. C. Chew, Y. G. Liu, and L. J. Jiang, "Generalized modal expansion of electromagnetic field in 2-D bounded and unbounded media," *IEEE Antennas Wireless Propag. Lett.*, vol. 11, pp. 1052–1055, 2012.

[16] Q. I. Dai, Y. H. Lo, W. C. Chew, Y. G. Liu, and L. J. Jiang, "Generalized modal expansion and reduced modal representation of 3-D electromagnetic fields," *IEEE Trans. Antennas Propag.*, vol. 62, no. 2, pp. 783–793, Feb. 2014.

[17] H. H. Gan, Q. I. Dai, T. Xia, Q. Liu, and W. C. Chew, "Reduced-order model with equivalence surface for scattering problems," *IEEE Antennas Wireless Propag. Lett.*, vol. 18, pp. 308–312, 2019.

[18] Q. I. Dai, W. C. Chew, and L. J. Jiang, "Differential-forms-motivated discretization of electromagnetic differential and integral equations," *IEEE Antennas Wireless Propag. Lett.*, vol 13, pp. 1223–1226, 2014.

[19] N. V. Venkatarayalu and J. F. Lee, "Removal of spurious DC modes in edges elements solutions for modeling three-dimensional resonators," *IEEE Trans. Microw. Theory Techn.*, vol. 54, no. 7, pp. 3019–3025, Jul. 2006.

[20] Q. Wu, "General metallic-dielectric structures a characteristic mode analysis using volume-surface formulations," *IEEE Antennas Propag. Mag.*, vol 65, no. 3, pp. 27–36, Jun. 2019.

[21] S. N. Makarov, G. M. Noetscher, and A. Nazarian, *Low-Frequency Electromagnetic Modeling for Electrical and Biological Systems Using Matlab*. Hoboken, NJ, USA: Wiley, 2015.